Proceedings of the ASME 2017 36th International Conference on Ocean, Offshore and Arctic Engineering
OMAE2017
June 25-30, 2017, Trondheim, Norway

OMAE2017-61688

ON INTERACTIONS BETWEEN WIND TURBINES AND THE MARINE BOUNDARY LAYER

M. Salman Siddiqui*
Department of Mathematical Sciences
NTNU
Alfred Getz vei 1
7491, Trondheim, Norway
Email: muhammad.siddiqui@math.ntnu.no

Adil Rasheed
CSE Group
Mathematics and Cybernetics
Sintef Digital
7034, Trondheim, Norway
Email: adil.rasheed@sintef.no

Mandar Tabib
CSE Group
Mathematics and Cybernetics
Sintef Digital
7034, Trondheim, Norway
Email: mandar.tabib@sintef.no

Eivind Fonn
CSE Group
Mathematics and Cybernetics
Sintef Digital
7034, Trondheim, Norway
Email: eivind.fonn@sintef.no

Trond Kvamsdal
Department of Mathematical Sciences
NTNU
Alfred Getz vei 1
7491, Trondheim, Norway
Email: trond.kvamsdal@math.ntnu.no

ABSTRACT

Most mesoscale models are developed with grid resolution in the range of kilometers. Therefore, they may require spatial averaging to analyze flow behavior over the domain of interest. In doing so, certain important features of sub-grid scales are lost. Moreover, spatial averaging on the governing equations results in additional terms known as dispersive fluxes. These fluxes are ignored in the analysis. The aim of this paper is to identify the significance of these fluxes for accurate assessment of flow fields related to wind farm applications. The research objectives are hence twofold: 1) to quantify the impact of wind turbines on MBL characteristics. 2) to account for the magnitude of dispersive fluxes arising from spatial averaging and make a comparison against the turbulent flux values. To conduct the numerical study the NREL 5MW reference wind turbine model is employed with a RANS approach using k-ε turbulence model. The results are presented concerning spatially averaged velocity, wake deficit behind the turbine, dispersive and turbulent fluxes.

.

NOMENCLATURE

ρ	Density(kg/m^3)
z_o	Surface roughness
Ω	Angular rotation rate(rad/sec)
$\overline{u_i}$	Spatially filtered velocity in tensor form(m/s)
$u^{'}$	Fluctuation in velocity with time(m/s)
CFD	Computational Fluid Dynamics
RANS	Reynolds Averaged Navier Stokes
BEM	Blade Element Momentum
LES	Large Eddy Simulation
MBL	Marine Boundary Layer
NREL	National Renewable Energy Laboratories

INTRODUCTION

With the size of operational offshore wind turbines increasing rapidly and already in the range of 100–150m, modeling of

*Address all correspondence to this author.

interactions between wind turbines and the MBL is becoming an important criterion to be taken into account during the design phase of wind turbines and farms. The thickness of the MBL can vary from $100m$ during the night to a few kilometers during the day. Closer to the surface variations in wind and temperature profiles are very sharp and can result in structural loads that can damage wind turbines or cause them to underperform [1]. Wind farms, on the other hand, can churn the lower part of the MBL and alter its characteristics. A good understanding of the interactions between each wind turbine, the wind farm, and the MBL is therefore of paramount importance [2]. The interactions can be understood either through experiments or numerical simulations [3]. The former approach is ruled out because the wind tunnel based conclusions can never be scaled to physical dimensions. It is also not economically feasible to conduct experiments due to the enormous size of existing megawatt wind turbines. Recently, with the current advances in computing [4, 5], the numerical approach using Computational Fluid Dynamics (CFD) to model flows around rotating structures beginning to receive significant attention.

The present paper deals with the utilization of a fully integrated CFD approach to simulate the MBL in the presence of a full-scale wind turbine. The NREL 5MW reference wind turbine model with a radius of $62.9m$ [6] is employed for the analysis and the MBL profiles are obtained using the empirical relations of field variables (U, k, ε). Performing numerical simulation on the entire wind farm requires a mesoscale model. However, such models do not have the necessary spatial grid resolution to simulate the appropriate sub-grid quantities directly. Hence parameterization is needed to model the effects produced by the stress contribution from sub-grid scale elements known as dispersive flux. Unlike the turbulent flux, these stresses are often neglected, which can significantly impact the overall performance of a whole wind farm.

We have used the k-ε turbulence model since it can be employed at a resolution which can explicitly resolve flow structures generated by wind turbines or buildings with affordable computational resources (approximately 100 times faster than large-eddy simulations) [7]. A reasonable agreement has been found with the BEM and LES results [8, 9]. The goal is to identify a general behavior of profiles rather than specific values at a point inside the domain; therefore results are evaluated regarding spatially averaged profiles of velocity, turbulent fluxes, and dispersive fluxes. In general, spatially averaged flow velocity shows that the turbine imparts a significant influence on the MBL profile, the major part of which is produced from the inner sections located near the blade hub. On the other hand, dispersive stress resulting from spatial averaging mesoscale equations highlight the significance against the turbulent stress.

TABLE 1. PARAMETRIZATION DETAIL FOR CAD MODEL OF WIND TURBINE BLADE

Profile	% Thickness	Begin radius	Chord	Twist
Cylinder1	100.0	2.00	3.542	0.000
Cylinder2	100.0	5.60	3.854	0.000
DU40	40.50	11.75	4.557	13.308
DU35	35.09	15.85	4.652	11.480
DU30	30.00	24.05	4.249	9.011
DU25	25.00	28.15	4.007	7.795
DU21	21.00	36.35	3.502	5.361
NACA64	18.00	44.55	3.010	3.125

APPROACH AND METHOD

CAD Model

For conducting high fidelity RANS simulations, the physical geometry of the 5MW NREL turbine is modeled. The wind turbine rotor is modeled using three $63m$ long blades defined in terms of cross-sectional profiles (DU21, DU25, DU30, DU35, DU40, and NACA64) and twist angles at different locations away from the hub [10]. The slight twist angle along the blade length helps to accommodate variations in relative wind velocity from root to tip. The details of the inherent characteristic of the CAD model are shown in Tab. 1.

Computational Mesh and Boundary Conditions

A finite element parametric mesh is generated with boundary layer prism elements near the blade boundary layer and unstructured polyhedral cells encompassing the rest of the domain. Additional layers of hexahedral elements are used near the ground. The mesh consists of 6 million cell elements. Inflow and outflow boundary conditions are applied on the inlet and exit faces of the domain respectively. On the turbine and ground surface, a no-slip boundary condition is applied for the velocity components, and a wall function is used to compute the boundary condition for the k and ε equations at the adjacent wall nodes. A slip boundary condition is applied on the vertical as well as the top surfaces of the domain as shown in Fig. 1. The domain is further divided into two zones: stationary and rotational. The rotational area includes the full turbine rotor and is more refined than the fixed domain. For all the examples in this work, we used the MBL conditions developed using Eqns. 1, 2 and 3 [11]. Within the bottom surface layer, the average variation in velocity is defined by the log profile about neutral conditions.

The free steam U_∞ at reference height is assu
$9m/s$.

$$u(z) = \frac{u_*}{\kappa}\left(ln\frac{z}{z_0}\right)$$
$$K(z) = C_\mu^{-1/2}u_*^2\left(1-\frac{z}{D}\right)$$
$$\varepsilon(z) = \frac{C_\mu^{0.75}K(z)^{1.5}}{\ell}; \qquad \ell = \frac{}{(1+}$$

where u_*, z_0, z and D represent friction veloc
ness, height above the ground surface and bou
ness, respectively. The constants have value
$C_\mu = 0.09$. The mean velocity is normalized
locity, given by u_τ, whereas the height is nor
fined as the height at which the surface velocity approaches zero. The rotational speed of the turbine is fixed at $\Omega = 10rpm$ to give a tip speed ratio (TSR) of 7.5. For all calculations, the reference fluid density is $\rho = 1.225kg/m^3$ and the dynamic viscosity is $\mu = 1.82\times10^{-}5kg/ms$ kg/ms are used for all the calculations. The Reynolds number is considered to be in the order of $\times10^6$, which is based on the average chord length of the cross sections located at 75% of the span [12]. The flow variables inside the domain are initialized using values equal to the inlet values. Before running the standard solver, an analytic solution is projected over the domain, which substantially increases the accuracy and convergence behavior. The computations are conducted at the time scale of $\times10^{-}4$. The time step size is originally based on the Courant number requirement, which keeps the solution within the accuracy limit [13].

Solver Details

The solver employed for the calculation of the velocity field along with modeled turbulent stress is based on Multiple Reference Frame (MRF) methodology and is created in OpenFOAM-2.3.0 (OF). To ensure continuity, OF uses an elliptic equation for the modified pressure which involves combining the continuity equation with the divergence of momentum equation. This elliptic equation, along with the momentum and turbulence equation, are solved in a segregated manner using the Semi-Implicit Method for Pressure-Linked Equations (SIMPLE) algorithm [14]. OpenFOAM uses a finite volume discretization technique; wherein all the equations are integrated over control volumes (CV) using the Green-Gauss divergence theorem. This doctrine converts the volume integral of the divergence of quantity into a surface integral over the boundary of the CV of the quantity itself. Thus, the divergence term defining the convection terms can be computed directly using the face values of variables in the CV. The face values of variables are obtained from their neighboring cell entered values by using a convective scheme. In

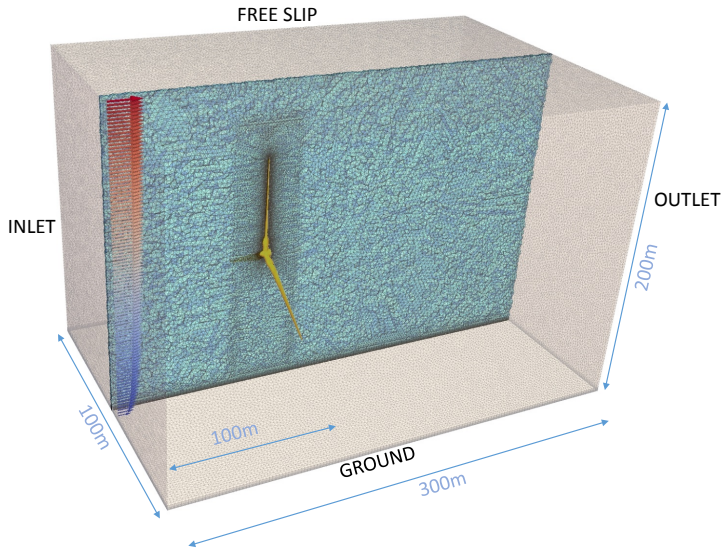

FIGURE 1. COMPUTATIONAL MODEL: DOMAIN, MESH, BOUNDARY CONDITIONS($4.7R \times 1.6R \times 3.1R$)

this work, all equations (except the k and turbulence equations) use a second order linear discretization scheme, while the turbulent equations use upwind convection schemes. Similarly, the diffusion term involving the Laplacian operator (the divergence of the gradient) is simplified to computing the gradient of the variable at the face. The gradient term can be split into contributions from the orthogonal part and the non-orthogonal parts, and both these contributions have been accounted for.

Multiple Reference Frames

The computational domain is divided into two zones; therefore two sets of governing equations are implemented. The rotational zone contains the turbine rotor, and it is modeled with the effects of rotation source terms in the form of Coriolis and Centrifugal forces. At the interface boundary, a transformation is applied to enable flow variables located inside one zone to be used to calculate fluxes at the boundary of the next zone [15]. In the stationary region, the following set of equations for mass and momentum are solved:

$$\frac{\partial u_i}{\partial x_i} = 0 \tag{4}$$
$$\frac{\partial (u_i u_j)}{\partial x_j} = -\frac{1}{\rho}\frac{\partial P}{\partial x_i} + \nu\frac{\partial^2 u_i}{\partial x_j^2} + Q \tag{5}$$

Where u is the absolute velocity as seen from a stationary reference frame. In the rotational zone, the same equations are rewritten in terms of the relative speed u (about the rotating frame of

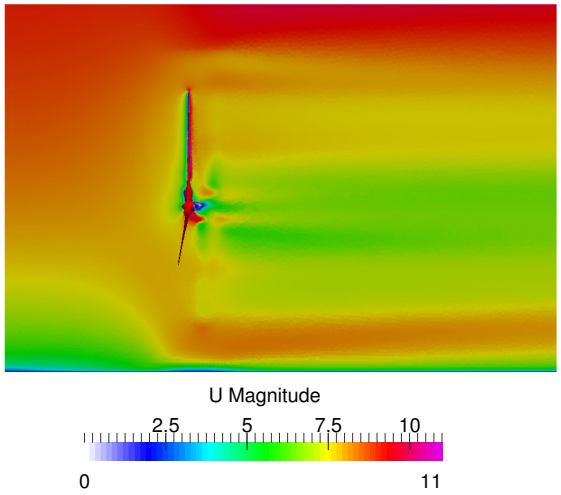

FIGURE 2. CONTOURS OF SPATIALLY AVERAGED VELOCITY MAGNITUDE

reference) given by:

$$\frac{\partial u_i}{\partial x_i} = 0 \tag{6}$$

$$\frac{\partial (u_i u_j)}{\partial x_j} + 2\Omega u_i + \Omega^2 r = -\frac{1}{\rho}\frac{\partial P}{\partial x_i} + \nu \frac{\partial^2 u_i}{\partial x_j^2} + Q \tag{7}$$

where the absolute and relative velocities are related by

$$u_a = u_r + \Omega \times r \tag{8}$$

Where Ω is the rotational speed of the reference frame with a stationary observer (here, equal to the rotational speed of the turbine), p is pressure, ν is the kinematic viscosity of the air and ν_t is the turbulent kinetic viscosity. This simulation methodology is robust and gives an accurate assessment of flow field for applications related to wind energy [5, 16].

PARAMETRIZATION OF MESOSCALE GOVERNING EQUATIONS IN WIND FARMS

To evaluate the results in terms of mesoscale modeling context of wind farms, we perform spatial averaging of the governing standard RANS equations that form the basis of a large variety of existing mesoscale codes [17]. The mass and momentum equations can be represented as:

$$\frac{\partial U_i}{\partial x_i} = 0 \tag{9}$$

$$\frac{\partial U_i}{\partial t} + \frac{\partial (U_i U_j)}{\partial x_j} + \frac{\partial (\overline{u_i' u_j'})}{\partial x_j} = -\frac{1}{\rho}\frac{\partial P}{\partial x_i} + \nu \frac{\partial^2 U_i}{\partial x_j^2} + Q \tag{10}$$

where U_i is the mean part of the velocity, u_i' the fluctuation of velocities in time, P mean pressure, $\overline{u_i' u_j'}$ the Reynolds stresses and Q the source term, which accounts for the coriolis and centrifqugal forces. Eq. 10 when averaged over space takes the following form:

$$\left\langle \frac{\partial U_i}{\partial t} \right\rangle + \left\langle \frac{\partial (U_i U_j)}{\partial x_j} \right\rangle + \left\langle \frac{\partial (\overline{u_i' u_j'})}{\partial x_j} \right\rangle = -\left\langle \frac{1}{\rho}\frac{\partial P}{\partial x_i} \right\rangle + \left\langle \nu \frac{\partial^2 U_i}{\partial x_j^2} \right\rangle + \langle Q \rangle \tag{11}$$

where angular brackets represent the space averaging operator. Such averaging will results in an additional system term called *dispersive flux*. We are interested in spatially averaged quantities which can be compared with the result of a mesoscale model grid. The values are computed by RANS simulations using MRF and a fine grid is employed. Considering that each grid point is representative of the volumetric average of the corresponding control volume, we applied Eq. 11 to the computational setup. The equation for the streamwise velocitny component can be expanded to the following form:

$$\frac{\partial \langle U \rangle}{\partial t} + \frac{\partial \langle UU \rangle}{\partial x} + \frac{\partial \langle UV \rangle}{\partial y} + \frac{\partial \langle UW \rangle}{\partial z} = \frac{\partial \langle \overline{u'u'} \rangle}{\partial x} + \frac{\partial \langle \overline{u'v'} \rangle}{\partial y} + \frac{\partial \langle \overline{u'w'} \rangle}{\partial z} - \frac{1}{\rho}\frac{\partial \langle P \rangle}{\partial x} + \nu \left\langle \frac{\partial^2 \langle \overline{U} \rangle}{\partial x^2} \right\rangle + \nu \left\langle \frac{\partial^2 \langle \overline{V} \rangle}{\partial y^2} \right\rangle + \nu \left\langle \frac{\partial^2 \langle \overline{W} \rangle}{\partial z^2} \right\rangle + \langle Q \rangle \tag{12}$$

As we have employed the steady state system of equations, we can neglect the first term on the left hand side. The second term on the left, using the flux divergence theorem, can be written as:

$$\left\langle \frac{\partial UU}{\partial x} \right\rangle = \frac{1}{V_{\text{air}}} \int_{V_{\text{air}}} \frac{\partial UU}{\partial x} \mathrm{d}v = \frac{1}{V_{\text{air}}} \int_S UU n_x \mathrm{d}s \tag{13}$$

Here V_{air} is the volume of air over which the averaging is performed, S is the surface delimiting the volume and n_x is the x-

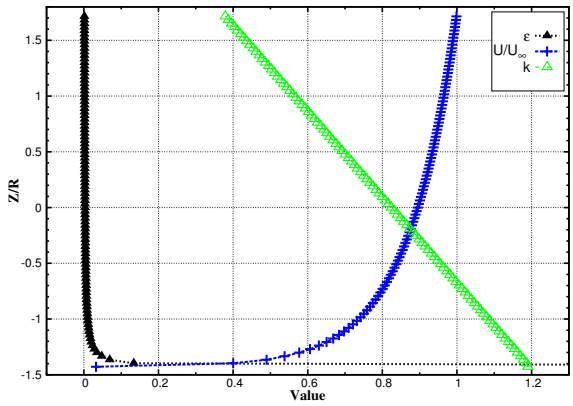

FIGURE 3. PROFILES OF MARINE BOUNDARY LAYER PARAMETERIZATION (U/U_∞, k, ε)

component of the normal pointing into the volume. For horizontal surfaces n_x is zero. Since we consider the case of fully developed flow, at the boundaries the contribution is zero, while over the surfaces of the turbine the velocity is also zero due to the no slip conditions. These assumptions eliminate the velocity contributions from the second and third term on left hand side, and also the first and second term on the right hand side of Eq. 12. Since the flow is considered turbulent, the viscous terms in the Eq. 12 (fifth, sixth and seventh) can also be neglected. This results in the following simplified equation:

$$\frac{\partial \langle \overline{u'w'} \rangle}{\partial z} + \frac{\partial \langle UW \rangle}{\partial z} + \frac{1}{\rho}\frac{\partial \langle P \rangle}{\partial x} = \langle Q \rangle \tag{14}$$

Splitting $U = \langle U \rangle + \tilde{u}$ and $W = \langle W \rangle + \tilde{w}$ where $\langle U \rangle$, $\langle W \rangle$ are spatially averaged velocity components and $\tilde{u}$ and $\tilde{w}$ are fluctuation in space, we get:

$$\langle UW \rangle = \langle U \rangle \langle W \rangle + \langle \tilde{u}\tilde{w} \rangle \tag{15}$$

Since, $\langle W \rangle = 0$ Eq. 15 reduces to $\langle UW \rangle = \langle \tilde{u}\tilde{w} \rangle$. Introducing this expression into Eq. 14 we obtain the following equation:

$$\frac{\partial \langle \overline{u'w'} \rangle}{\partial z} + \frac{\partial \langle \tilde{u}\tilde{w} \rangle}{\partial z} + \frac{1}{\rho}\frac{\partial \langle P \rangle}{\partial x} = \langle Q \rangle \tag{16}$$

The first and second terms on the left are the gradients in the vertical direction of turbulent and dispersive fluxes respectively. The third term is the gradient of pressure in the flow direction. To study the vertical profiles of the streamwise velocity, Reynolds shear stress, and dispersive stress we evaluate these quantities

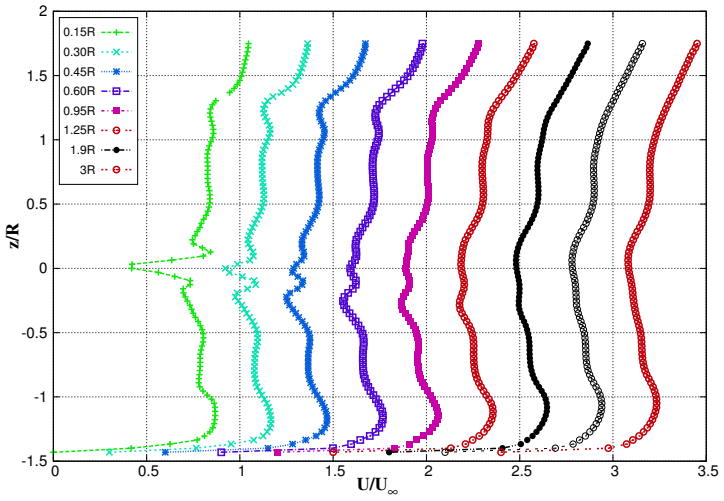

FIGURE 4. TURBINES EFFECT ON MBL CHARACTERISTICS AT VARIOUS STATIONS IN DOWNSTREAM DIRECTION

from the result obtained from the simulation using Eqns. 17 through 20.

$$\langle U \rangle_k = \frac{\sum_i \sum_j (U)_{i,j} V_{i,j}}{\sum_i \sum_j V_{i,j}} \tag{17}$$

$$\langle \tilde{u}\tilde{w} \rangle_k = \frac{\sum_i \sum_j (\tilde{u}\tilde{w})_{i,j} V_{i,j}}{\sum_i \sum_j V_{i,j}} \tag{18}$$

$$\langle \overline{u'w'} \rangle_k = \frac{\sum_i \sum_j (\overline{u'w'})_{i,j} V_{i,j}}{\sum_i \sum_j V_{i,j}} \tag{19}$$

$$\langle \mathrm{TKE} \rangle_k = \frac{\sum_i \sum_j (\mathrm{TKE})_{i,j} V_{i,j}}{\sum_i \sum_j V_{i,j}} \tag{20}$$

Results and Discussion

Mean Velocity Profiles

To model MBL characteristics inside the atmosphere, vertical profiles employed for the distribution of turbulent kinetic energy, dissipation rate and flow velocity are developed from the empirical relationships given by Eqns. 1, 2 and 3. Since velocity variations follow a logarithmic pattern above the surface, a log expression is used to model the flow distribution in the computational domain. High shear production near the ground causes large turbulent transport of momentum between adjacent layers, which is incorporated by employing variable profiles for turbulent kinetic energy and dissipation rate (Fig. 3).

During turbine operation, the incoming flow transfers its momentum to the blades of the rotor, causing significant variation in the characteristics of the MBL. A reduced velocity (wake)

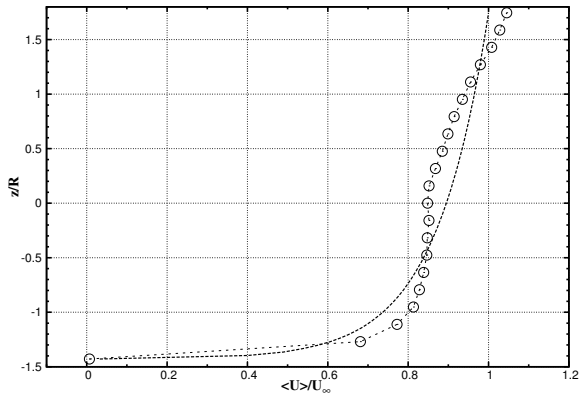

FIGURE 5. SPATIALLY AVERAGED VELOCITY DISTRIBUTION OVER THE DOMAIN: AFTER CONVERGENCE (- - -), WITHOUT TURBINE OPERATION (o o o)

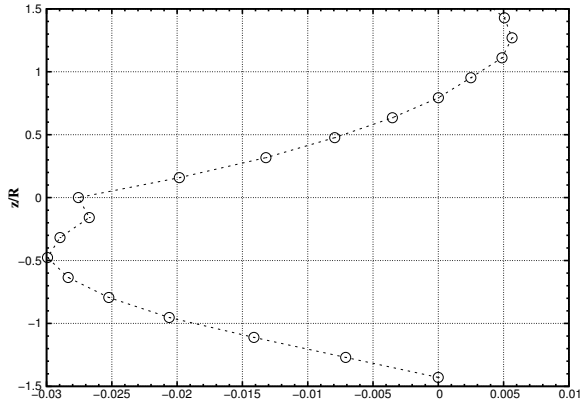

FIGURE 6. SPATIALLY AVERAGED TURBULENT FLUX $\langle \overline{u'w'} \rangle$

behind the turbine is visible from Fig. 2, which depicts the distribution of the flow field on a two-dimensional plane in the streamwise direction. The reduction shows the impact of the turbine on MBL characteristics in the downstream direction. To quantitatively study the effect, velocity profiles in the vertical direction are plotted at distances of 0.15R, 0.30R, 0.45R, 0.60R, 0.95R, 1.25R, 1.9R and 3R in the streamwise direction from the rotor center. It can be seen from Fig. 4 that significant impact on MBL is produced from the center of rotor hub, and moving downstream (approximately 0.15R–0.3R) this reduces from almost 20% to 5%. Overall, the wake profiles extracted adjacent to the rotor show more dramatic reduction in velocity along with oscillatory behavior. Considering the sudden changes in flow due to large vortices and adverse pressure gradients (see Fig. 2), this prediction looks reasonable.

To identify the overall magnitude of the influence of field variables, the spatially averaged streamwise velocity is plotted in Fig. 5. It can be seen that the flow velocity follows a logarithmic pattern from the ground surface up to the lower edge of the blade, beyond which the shape becomes influenced by the operation of the rotor. Within limits of rotor diameter, the wake velocity first decreases in the vertical direction until center of the rotor, after which it starts to increase again. This uneven distribution of MBL characteristics is considered to be due to the variable distribution of flow velocity [16]. Higher velocities in the upper half of turbine rotor lead to quick wake recovery and leave small footprints on MBL in contrast to the lower side of the rotor. Subsequently, the logarithmic variation of flow velocity is again observed from rotor top until the end of the computational domain.

Turbulent Stresses

The modeled stress from RANS simulations are plotted in Fig. 6, which depicts the spatially averaged distribution of the turbulent part of the stress in the vertical direction. It is a direct measure of turbulence present in the flow. Currently, the concentration of turbulent stress is found mostly in regions occupied by the rotor, whereas, on either side of the rotor a lower magnitude of turbulent stress is observed in the horizontal direction. It represents a reduced transport of momentum due to less turbulence.

During turbine operation turbulent stress is observed to have negative values, which implies the presence of down gradient flux. Within the area encompassing rotor diameter, turbulent fluxes decrease with height until the center of the rotor where a minimum is observed, and after that, the magnitude starts to increase again towards the upper edge of the rotor. Unlike dispersive fluxes, turbulent flux does not approach zero at the end of rotor edge. However, its magnitude becomes first positive after which the profile pattern is such that it starts to become zero. These stresses exactly approach zero at the height of $\approx 1R$ from the top of the rotor edge, which implies a little sign of turbulence in the region. The reason why turbulent fluxes do not approach zero at the rotor tip is due to the expansion of wakes width downstream of the turbine. Therefore, turbulent fluctuations upon averaging are still observed from the rotor top until the end of the computational domain. The expansion is also visible from Fig. 4, which corresponds to turbulent stress values in the vertical direction.

Dispersive Stresses

Dispersive stresses are neglected in mesoscale models. A quantitative comparison of dispersive stress against turbulent stress is provided in this section to highlight its significance in making an accurate assessment of total stress values. It can be seen from Fig. 7 that the magnitude of dispersive terms is comparable to turbulent ones, however, near the ground surface they

produce an insignificant contribution to total stress value. In the vertical direction, dispersive stress first increases and reaches a maximum value towards rotor center, after which it starts to reduce again and vanish completely at the rotor top. The turbulent fluxes are given in Fig. 6 shows negative values within the area encompassed by the turbine. Similar magnitudes of dispersive fluxes are found in the spanwise direction; however, their positive values imply that the flux is a counter-gradient. The dispersive flux approaches zero at the top of the rotor, unlike to the turbulent stress profile shown in the previous section. The shape of the dispersive flux pattern is in agreement with those modeled by [18, 19]. However, they have incorporated different configurations of cubes array using CFD. Maxima for dispersive stress for the cited authors are located at the top of buildings, whereas in the present case of wind turbines, the maxima are achieved at the center of the turbine. A similar trend is observed for regard to turbulent stresses. To better understand the pattern of dispersive flux we plotted the streamlines of velocity on a 2D plane located at the center of the rotor in the lateral direction in Fig. 8. As dispersive flux is defined as $\tilde{u}\tilde{w} = (\langle U \rangle - U)(\langle W \rangle - W)$, where the trend of the profile shape depends on the sign of $\tilde{u}$ and $\tilde{w}$. The flow in the streamwise direction ($\langle U \rangle$) once averaged over the entire domain repeatedly results in a positive value. On the other hand, behind the turbine, due to vortex formation, there are regions where U becomes negative which imply that $\tilde{u}$ remains consistently positive. Hence, the magnitude of dispersive flux depends on the sign of $\tilde{w}$. Considering $\langle W \rangle$ is negligible one can conclude that the sign of $\tilde{w}$ will determine the overall pattern of the profile. As the flow becomes fully developed with turbine rotating in a clockwise manner, the wind is deflected downwards and generates vortices that are spinning behind the hub with both negative and positive values of U in the streamwise direction. On the top and bottom the values are positive for U due to the input parameterization of field variables. However, due to down gradient flux, the magnitude of the negative effect of $\tilde{w}$ is larger. Hence, the product $\tilde{u}\tilde{w}$ becomes positive during the averaging procedure, and a positive overall trend of dispersive flux values is observed.

CONCLUSION

The NREL 5MW reference wind turbine rotor was employed, with a chosen set of parameters to develop an accurate representation of MBL conditions in the domain. RANS analysis with k-ε model was performed to compute flow variables using MRF computational methodology. Numerical methods were first validated with the BEM and LES investigations found in the literature [8, 9, 12]. Using numerical studies, spatially averaged distribution of flow velocity, turbulent and dispersive flux were calculated. It was found that the presence of the rotor alters the characteristics of the MBL profile significantly. On either side of the rotor (above and below), a logarithmic variation

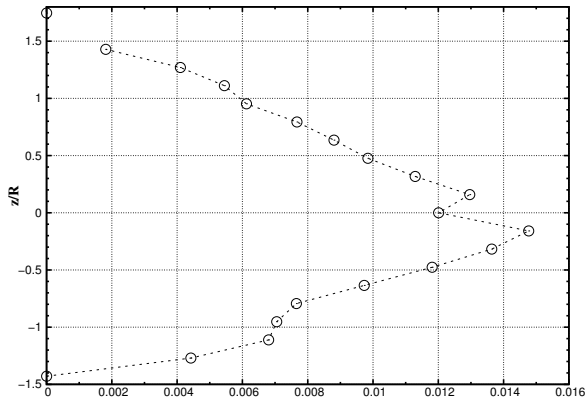

FIGURE 7. SPATIALLY AVERAGED DISPERSIVE FLUX $\langle \tilde{u}\tilde{w} \rangle$

of spatially averaged flow velocity was found, whereas within the region occupied by rotor a reduced velocity pattern was observed. This reduced velocity first decreases towards the center of the rotor and achieved a minimum, after which it started to increase again. Horizontal homogenization (spatial averaging) of the Navier-Stokes equations was also performed to see the influence of additional terms coming from the mesoscale code in wind farm applications. The homogenization process results in other terms called dispersive fluxes. The spatially averaged distribution of turbulent and dispersive stresses was quantified, and a comparable contribution was found from the former in comparison to the latter. Furthermore, the input from dispersive fluxes become zero at the rotor edge, whereas turbulent stresses reach zero after a distance of approximately $1R$ due to the increase in the wake width in the downstream direction. Hence, it can be concluded that dispersive flux should be taken into consideration when making an accurate representation of total stresses in a mesoscale model.

ACKNOWLEDGMENT

The authors acknowledge the financial support from the Norwegian Research Council and the industrial partners of NOWITECH: Norwegian Research Centre for Offshore Wind Technology (Grant No.:193823/S60) (http://www.nowitech.no) and FSI-WT (Grant No.:216465/E20)(http://www.fsi-wt.no). Furthermore, the authors greatly acknowledge the Norwegian Metacenter for Computational Science (NOTUR-reference number: NN9322K/1589) (www.notur.no) for giving us access to the Vilje high-performance computer at the Norwegian University of Science and Technology (NTNU).

REFERENCES

[1] Drenkmper, M., Witha, B., Steinfeld, G., Heinemann, D., and Khn, M., 2015. "The impact of stable atmospheric

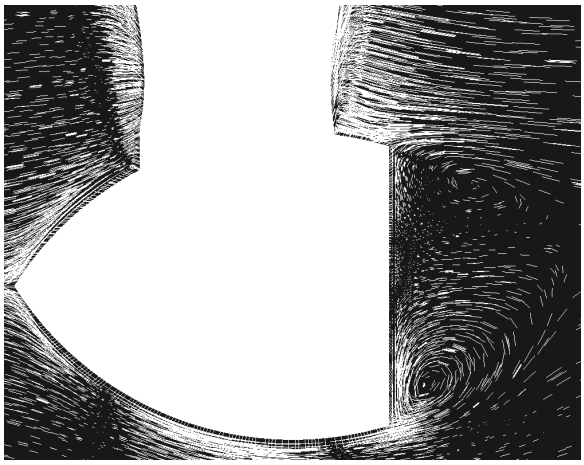

FIGURE 8. STREAMLINES OF VELOCITY AT MIDPLANE (X-Z)

boundary layers on wind-turbine wakes within offshore wind farms". *Journal of Wind Engineering and Industrial Aerodynamics,* ***144***, pp. 146 – 153.

[2] Agel, F. P., Wu, Y. T., Lu, H., and Conzemius, R. J., 2011. "Large-eddy simulation of atmospheric boundary layer flow through wind turbines and wind farms". *Journal of Wind Engineering and Industrial Aerodynamics,* ***99***(4), pp. 154 – 168.

[3] Siddiqui, M. S., Durrani, N., and Akhtar, I., 2015. "Quantification of the effects of geometric approximations on the performance of a vertical axis wind turbine". *Renewable Energy,* ***74***(0), pp. 661–670.

[4] Wu, Y. T., and Agel, F. P., 2015. "Modeling turbine wakes and power losses within a wind farm using les: An application to the *H*orns *R*ev offshore wind farm". *Renewable Energy,* ***75***, pp. 945 – 955.

[5] Siddiqui, M. S., Rasheed, A., Tabib, M., and Kvamsdal, T., 2016. "Numerical analysis of nrel 5*MW* wind turbine: A study towards a better understanding of wake characteristic and torque generation mechanism". *Journal of Physics: Conference Series,* ***753***(3), p. 032059.

[6] Kooijman, H. J. T., Lindenburg, C., Winkelaar, D., , and Hooft, E. L. V. D., 2003. "Dowec 6 MW pre-design: Aero-elastic modeling of the dowec 6 MW pre-design in phatas,". *DOWEC Dutch Offshore Wind Energy Converter 19972003 Public Reports , DOWEC 10046-009, ECN-CX–01-135, Petten, the Netherlands: Energy Research Center of the Netherlands*.

[7] Cheng, Y., Lien, F., Yee, E., and Sinclair, R., 2003. "A comparison of large eddy simulations with a standard k reynolds-averaged navierstokes model for the prediction of a fully developed turbulent flow over a matrix of cubes". *Journal of Wind Engineering and Industrial Aerodynamics,* ***91***(11), pp. 1301 – 1328.

[8] Jonkman, J., Marshal, L., and Buhl, J., 2005, Tech. Rep. NREL/EL-500-38230. "FAST users guide.". *National Renewable Energy Laboratory, Golden, CO,*.

[9] Hsu, M. C., and Bazilevs, Y., 2012. "Fluid–structure interaction modeling of wind turbines: simulating the full machine". *Computational Mechanics,* ***50***(6), pp. 821–833.

[10] Jonkman, J. M., Butterfield, S., Musial, W., and Scott, G., 2009, Tech. Rep. NREL/TP-500e38060. "Definition of a 5MW reference wind tturbine for offshore system development.". *National Renewable Energy Laboratory*.

[11] Tabib, M., Rasheed, A., and Kvamsdal, T., 2015. "Investigation of the impact of wakes and stratification on the performance of an onshore wind farm". *Energy Procedia,* ***80***, pp. 302 – 311. 12th Deep Sea Offshore Wind Energy Conference, *EERA* DeepWind 2015.

[12] Bazilevs, Y., Hsu, M. C., Akkerman, I., Wright, S., Takizawa, K., Henicke, B., Spielman, T., and Tezduyar, T. E., 2011. "3D simulation of wind turbine rotors at full scale. part *I*: Geometry modeling and aerodynamics". *International Journal for Numerical Methods in Fluids,* ***65***(1-3), pp. 207–235.

[13] Siddiqui, M. S., Durrani, N., and Akhtar, I., 2013. "Numerical study to quantify the effects of struts and central hub on the performance of a three dimensional vertical axis wind turbine using sliding mesh". *ASME Power Conference,* ***2***(POWER2013-98300), p. V002T09A020(11).

[14] Siddiqui, M. S., Durrani, N., and Akhtar, I., 2013. "Numerical study to quantify the effects of struts and central hub on the performance of a three dimensional vertical axis wind turbine using sliding mesh". *ASME Power Conference,* ***2***(POWER2013-98300), p. V002T09A020(11).

[15] Jasak, H., 5-8 January, 2008. "Dynamic mesh handling in openfoam". *47th AIAA Aerospace Sciences Meeting Including the New Horizons Forum and Aerospace Exposition,* ***52***, pp. (AIAA 2009–341).

[16] Siddiqui, M. S., Rasheed, A., Tabib, M., and Kvamsdal, T., 9-13 January, 2017. "Numerical modeling framework for wind turbine analysis and atmospheric boundary layer interaction". *35th Wind Energy Symposium, AIAA SciTech*, p. (AIAA 2548594).

[17] Gopalan, H., Gundling, C., Brown, K., Roget, B., Sitaraman, J., Mirocha, J. D., and Miller, W. O., 2014. "A coupled mesoscalemicroscale framework for wind resource estimation and farm aerodynamics". *Journal of Wind Engineering and Industrial Aerodynamics,* ***132***(0), pp. 13–26.

[18] Martilli, A., and Santiago, J. L., 2007. "Cfd simulation of airflow over a regular array of cubes. part ii: analysis of spatial average properties". *Boundary-Layer Meteorology,* ***122***(3), pp. 635–654.

[19] Rasheed, A., and Robinson, D., 2013. "Characterization of dispersive fluxes in mesoscale models using *LES* of flow

over an array of cubes". *International Journal of Atmospheric Sciences,* ***2013***(898095).